7 Displacement of reference points (19 June 2015)

Models describing the displacements of reference points due to various effects are provided. In the following, three kinds of displacements are distinguished:

- Conventional displacements of reference markers on the crust (see Section 7.1) relate the regularized positions $X_R(t)$ of the reference points (see Chapter 4) to their conventional instantaneous positions. Generally these conventional instantaneous positions are used in data analyses as *a priori* coordinates for subsequent adjustment of observational data. They include tidal motions (mostly near diurnal and semidiurnal frequencies) and other accurately modeled displacements of reference markers (mostly at longer periods);
- Other displacements of reference markers (Section 7.2, presently, at the time of publication, under development) include non-tidal motions associated with changing environmental loads (very broad spectral content);
- Displacements that affect the internal reference points within the observing instruments, which are generally technique-dependent, are mentioned in Section 7.3.

The first two categories of displacements are described by geophysical models or gridded convolution results derived from geophysical models. The last category includes empirical physical effects that have been demonstrated to affect geodetic observing instruments.

As the non-tidal load displacements (Section 7.2) normally change very little over typical integration spans and because models for these effects are usually less accurate, it is generally recommended that they *not* be included in computing conventional instantaneous positions. Instead, the corresponding non-tidal loading effects will remain as signals embedded in the geodetic time series results. These signals can be extracted and compared with the model results referenced here in post-analysis studies.

In combinations of diverse analysis results, it is particularly important that equivalent displacement models are applied for like effects. Non-tidal load displacements should be consistently excluded from the conventional instantaneous positions, as recommended here, or else the same geophysical loading models together with the same environmental inputs should be applied.

7.1 Models for conventional displacement of reference markers on the crust

This section describes conventional models for displacement due to the body tides arising from the direct effect of the external tide generating potential (7.1.1), displacement due to ocean tidal loading (7.1.2) and due to diurnal and semidiurnal atmospheric pressure loading (7.1.3), displacement due to the centrifugal perturbations caused by Earth rotation variations, including the pole tide (7.1.4) and the loading caused by the ocean pole tide (7.1.5).

7.1.1 Effects of the solid Earth tides

7.1.1.1 *Conventional model for solid Earth tides*

Site displacements caused by tides of spherical harmonic degree and order (nm) are characterized by the Love number h_{nm} and the Shida number l_{nm}. The effective values of these numbers depend on station latitude and tidal frequency (Wahr, 1981). The latitude dependence and a small interband variation are caused by the Earth's ellipticity and the Coriolis force due to Earth rotation. A strong frequency dependence within the diurnal band is produced by the Nearly Diurnal Free Wobble resonance associated with the FCN in the wobbles of the Earth and its core regions which contribute to the tidal deformations via their centrifugal effects. Additionally, the resonance in the deformation due to ocean tidal loading, which is not included in the computations of the last section which use constant load Love numbers, may be represented in terms of effective contributions to h_{21} and l_{21}. A further frequency dependence, which is most pronounced in the long-period tidal band, arises from mantle anelasticity leading to corrections to the elastic Earth Love numbers. The contributions to

the Love number parameters from anelasticity and ocean tidal loading as well as those from the centrifugal perturbations due to the wobbles have imaginary parts which cause the tidal displacements to lag slightly behind the tide generating potential. All these effects need to be taken into account when an accuracy of 1 mm is desired in determining station positions.

In order to account for the latitude dependence of the effective Love and Shida numbers, the representation in terms of multiple h and l parameters employed by Mathews *et al.* (1995) is used. In this representation, parameters $h^{(0)}$ and $l^{(0)}$ play the roles of h_{2m} and l_{2m}, while the latitude dependence is expressed in terms of additional parameters $h^{(2)}, h'$ and $l^{(1)}, l^{(2)}, l'$. These parameters are defined through their contributions to the site displacement as given by equations (1a-1c) below. Their numerical values as listed in the Conventions 1996 have since been revised, and the new values presented in Table 7.2 are used here. These values pertain to the elastic Earth and anelasticity models referred to in Chapter 6.

The vector displacement $\Delta\vec{r}_f$ due to a tidal term of frequency f is given by the following expressions that result from evaluation of the defining equation (2) of Mathews *et al.* (1995):

For a long-period tide of frequency f:

$$\begin{aligned}\Delta\vec{r}_f \;=\; \sqrt{\tfrac{5}{4\pi}}H_f \;\Bigg\{ & \left[h(\phi)\left(\tfrac{3}{2}\sin^2\phi - \tfrac{1}{2}\right) + \sqrt{\tfrac{4\pi}{5}}h'\right]\cos\theta_f\ \hat{r} \\ & +3l(\phi)\sin\phi\cos\phi\cos\theta_f\ \hat{n} \\ & +\cos\phi\ \left[3l^{(1)}\sin^2\phi - \sqrt{\tfrac{4\pi}{5}}l'\right]\sin\theta_f\ \hat{e}\Bigg\}.\end{aligned} \tag{1a}$$

For a diurnal tide of frequency f:

$$\begin{aligned}\Delta\vec{r}_f \;=\; -\sqrt{\tfrac{5}{24\pi}}H_f \;\Bigg\{ & h(\phi)3\sin\phi\cos\phi\sin(\theta_f+\lambda)\ \hat{r} \\ & +\left[3l(\phi)\cos 2\phi - 3l^{(1)}\sin^2\phi + \sqrt{\tfrac{24\pi}{5}}l'\right]\sin(\theta_f+\lambda)\ \hat{n} \\ & +\left[\left(3l(\phi) - \sqrt{\tfrac{24\pi}{5}}l'\right)\sin\phi - 3l^{(1)}\sin\phi\cos 2\phi\right]\cos(\theta_f+\lambda)\ \hat{e}\Bigg\}.\end{aligned} \tag{1b}$$

For a semidiurnal tide of frequency f:

$$\begin{aligned}\Delta\vec{r}_f \;=\; \sqrt{\tfrac{5}{96\pi}}H_f \;\Bigg\{ & h(\phi)3\cos^2\phi\cos(\theta_f+2\lambda)\ \hat{r} \\ & -6\sin\phi\cos\phi\left[l(\phi)+l^{(1)}\right]\cos(\theta_f+2\lambda)\ \hat{n} \\ & -6\cos\phi\left[l(\phi)+l^{(1)}\sin^2\phi\right]\sin(\theta_f+2\lambda)\ \hat{e}\Bigg\}.\end{aligned} \tag{1c}$$

In the above expressions,

$$\begin{aligned} h(\phi) &= h^{(0)} + h^{(2)}(3\sin^2\phi - 1)/2, \\ l(\phi) &= l^{(0)} + l^{(2)}(3\sin^2\phi - 1)/2, \end{aligned} \tag{2}$$

H_f = amplitude (m) of the tidal term of frequency f,

ϕ = geocentric latitude of station,

λ = east longitude of station,

θ_f = tide argument for tidal constituent with frequency f,

$\hat{r}$ = unit vector in radial direction,

$\hat{e}$ = unit vector in east direction,

$\hat{n}$ = unit vector perpendicular to $\hat{r}$ in the northward direction.

The convention used in defining the tidal amplitude H_f is the one from Cartwright and Tayler (1971). To convert amplitudes defined according to other conventions that have been employed in recent more accurate tables, use the conversion factors given in Chapter 6, Table 6.8.

Equations (1) assume that the Love and Shida number parameters are all real. Generalization to the case of complex parameters is done simply by making the following replacements for the combinations $L\cos(\theta_f + m\lambda)$ and $L\sin(\theta_f + m\lambda)$, wherever they occur in those equations:

$$L\cos(\theta_f + m\lambda) \to L^R\cos(\theta_f + m\lambda) - L^I\sin(\theta_f + m\lambda), \tag{3a}$$

$$L\sin(\theta_f + m\lambda) \to L^R\sin(\theta_f + m\lambda) + L^I\cos(\theta_f + m\lambda), \tag{3b}$$

where L is a generic symbol for $h^{(0)}, h^{(2)}, h', l^{(0)}, l^{(1)}, l^{(2)}$, and l', and where L^R and L^I stand for their respective real and imaginary parts.

The complex values of these 7 parameters are computed for the diurnal body tides from resonance formulae of the form given in Equation (9) of Chapter 6 using the values listed in Equation (10) of that chapter for the resonance frequencies σ_α and those listed in Table 7.1 for the coefficients L_0 and L_α relating to each of the multiple h and l Love/Shida numbers. The manner in which σ_α and L_α were computed is explained in Chapter 6, where mention is also made of the models used for the elastic Earth and for mantle anelasticity. As was noted in that chapter, the frequency dependence of the ocean tide contributions to certain Earth parameters in the equations of motion for the wobbles has the effect of making the resonance formulae inexact. The difference between the exact and resonance formula values is included in the tabulated values of $h_{21}^{(0)}$ and $l_{21}^{(0)}$ in Table 7.2. (The only case where this difference makes a contribution above the cut-off in Table 7.3a is in the radial displacement due to the ψ_1 tide.) Also included in the values listed in Table 7.2 are the resonant ocean tidal loading corrections outlined in the next paragraph.

Table 7.1: Parameters in the resonance formulae for the displacement Love numbers.

	$h^{(0)}$		$h^{(2)}$	
α	Re L_α	Im L_α	Re L_α	Im L_α
0	$.60671 \times 10^{+0}$	$-.2420 \times 10^{-2}$	$-.615 \times 10^{-3}$	$-.122 \times 10^{-4}$
1	$-.15777 \times 10^{-2}$	$-.7630 \times 10^{-4}$	$.160 \times 10^{-5}$	$.116 \times 10^{-6}$
2	$.18053 \times 10^{-3}$	$-.6292 \times 10^{-5}$	$.201 \times 10^{-6}$	$.279 \times 10^{-8}$
3	$-.18616 \times 10^{-5}$	$.1379 \times 10^{-6}$	$-.329 \times 10^{-7}$	$-.217 \times 10^{-8}$
	$l^{(0)}$		$l^{(1)}$	
α	Re L_α	Im L_α	Re L_α	Im L_α
0	$.84963 \times 10^{-1}$	$-.7395 \times 10^{-3}$	$.121 \times 10^{-2}$	$.136 \times 10^{-6}$
1	$-.22107 \times 10^{-3}$	$-.9646 \times 10^{-5}$	$-.316 \times 10^{-5}$	$-.166 \times 10^{-6}$
2	$-.54710 \times 10^{-5}$	$-.2990 \times 10^{-6}$	$.272 \times 10^{-6}$	$-.858 \times 10^{-8}$
3	$-.29904 \times 10^{-7}$	$-.7717 \times 10^{-8}$	$-.545 \times 10^{-8}$	$.827 \times 10^{-11}$
	$l^{(2)}$		l'	
α	Re L_α	Im L_α	Re L_α	Im L_α
0	$.19334 \times 10^{-3}$	$-.3819 \times 10^{-5}$	$-.221 \times 10^{-3}$	$-.474 \times 10^{-7}$
1	$-.50331 \times 10^{-6}$	$-.1639 \times 10^{-7}$	$.576 \times 10^{-6}$	$.303 \times 10^{-7}$
2	$-.66460 \times 10^{-8}$	$.5076 \times 10^{-9}$	$.128 \times 10^{-6}$	$-.378 \times 10^{-8}$
3	$.10372 \times 10^{-7}$	$.7511 \times 10^{-9}$	$-.655 \times 10^{-8}$	$-.291 \times 10^{-9}$

2015/06/19

Site displacements caused by solid Earth deformations due to ocean tidal loading are dealt with in section 7.1.2. Constant nominal values are assumed for the load Love numbers in computing these. The values used for tides of degree 2 are $h_2'^{(nom)}$ = -1.001, $l_2'^{(nom)} = 0.0295$, $k_2'^{(nom)}$ = -0.3075. Since resonances in the diurnal band also cause the values of the load Love numbers to vary, corrections need to be applied to the results of section 7.1.2. These corrections can be expressed in terms of effective ocean tide contributions $\delta h^{(OT)}$ and $\delta l^{(OT)}$ to the respective body tide Love numbers $h_{21}^{(0)}$ and $l_{21}^{(0)}$. $\delta h^{(OT)}$ and $\delta l^{(OT)}$ are given by expressions of the form (11) of Chapter 6, with appropriate replacements. They were computed using the same ocean tide admittances as in that chapter, and using the resonance parameters listed in Table 6.4 for the load Love numbers; they are included in the values listed in Table 7.2 under $h^{(0)R}$ and $h^{(0)I}$ for the diurnal tides.

The variation of $h_{20}^{(0)}$ and $l_{20}^{(0)}$ across the zonal tidal band, ($nm = 20$), due to mantle anelasticity, is described by the formulae

$$h_{20}^{(0)} = 0.5998 - 9.96 \times 10^{-4} \left\{ \cot \frac{\alpha\pi}{2} \left[1 - \left(\frac{f_m}{f} \right)^{\alpha} \right] + i \left(\frac{f_m}{f} \right)^{\alpha} \right\}, \tag{4a}$$

$$l_{20}^{(0)} = 0.0831 - 3.01 \times 10^{-4} \left\{ \cot \frac{\alpha\pi}{2} \left[1 - \left(\frac{f_m}{f} \right)^{\alpha} \right] + i \left(\frac{f_m}{f} \right)^{\alpha} \right\} \tag{4b}$$

on the basis of the anelasticity model already referred to. Here f is the frequency of the zonal tidal constituent, f_m is the reference frequency equivalent to a period of 200 s, and $\alpha = 0.15$.

Table 7.2 lists the values of $h^{(0)}, h^{(2)}, h', l^{(0)}, l^{(1)}, l^{(2)}$, and l' for those tidal frequencies for which they are needed for use in the computational procedure described below. The tidal frequencies shown in the table are given in cycles per sidereal day (cpsd). Periods, in solar days, of the nutations associated with the diurnal tides are also shown.

Computation of the variations of station coordinates due to solid Earth tides, like that of geopotential variations, is done most efficiently by the use of a two-step procedure. The evaluations in the first step use the expression in the time domain for the full degree 2 tidal potential or for the parts that pertain to particular bands ($m = 0, 1,$ or 2). Nominal values common to all the tidal constituents involved in the potential and to all stations are used for the Love and Shida numbers h_{2m} and l_{2m} in this step. They are chosen with reference to the values in Table 7.2 so as to minimize the computational effort needed in Step 2. Along with expressions for the dominant contributions from $h^{(0)}$ and $l^{(0)}$ to the tidal displacements, relatively small contributions from some of the other parameters are included in Step 1 for reasons of computational efficiency. The displacements caused by the degree 3 tides are also computed in the first step, using constant values for h_3 and l_3.

Corrections to the results of the first step are needed to take account of the frequency-dependent deviations of the Love and Shida numbers from their respective nominal values, and also to compute the out-of-phase contributions from the zonal tides. Computations of these corrections constitute Step 2. The total displacement due to the tidal potential is the sum of the displacements computed in Steps 1 and 2.

The full scheme of computations is outlined in the chart on page 6.

Table 7.2: Displacement Love number parameters for degree 2 tides. Superscripts R and I identify the real and imaginary parts, respectively. Periods are given in solar days and frequencies in cpsd.

Name	Period	Frequency	$h^{(0)R}$	$h^{(0)I}$	$h^{(2)}$	h'
Semidiurnal		-2	.6078	-.0022	-.0006	
Diurnal						
$2Q_1$	6.86	0.85461	.6039	-.0027	-.0006	
σ_1	7.10	0.85946	.6039	-.0026	-.0006	
135,645	9.12	0.89066	.6036	-.0026	-.0006	
Q_1	9.13	0.89080	.6036	-.0026	-.0006	
ρ_1	9.56	0.89565	.6035	-.0026	-.0006	
145,545	13.63	0.92685	.6028	-.0025	-.0006	
O_1	13.66	0.92700	.6028	-.0025	-.0006	
τ_1	14.77	0.93246	.6026	-.0025	-.0006	
$N\tau_1$	23.94	0.95835	.6011	-.0024	-.0006	
No_1	27.55	0.96381	.6005	-.0023	-.0006	
χ_1	31.81	0.96865	.5998	-.0023	-.0006	
π_1	121.75	0.99181	.5878	-.0015	-.0006	
P_1	182.62	0.99454	.5817	-.0011	-.0006	
S_1	365.26	0.99727	.5692	-.0004	-.0006	
165,545	6798.38	0.99985	.5283	.0023	-.0007	
K_1	infinity	1.00000	.5236	.0030	-.0007	
165,565	-6798.38	1.00015	.5182	.0036	-.0007	
165,575	-3399.19	1.00029	.5120	.0043	-.0007	
ψ_1	-365.26	1.00273	1.0569	.0036	-.0001	
166,564	-346.64	1.00288	.9387	-.0050	-.0003	
ϕ_1	-182.62	1.00546	.6645	-.0059	-.0006	
θ_1	-31.81	1.03135	.6117	-.0030	-.0006	
J_1	-27.55	1.03619	.6108	-.0030	-.0006	
Oo_1	-13.66	1.07300	.6080	-.0028	-.0006	
Long period						
55,565	6798.38	.000147	.6344	-.0093	-.0006	.0001
S_{sa}	182.62	.005461	.6182	-.0054	-.0006	.0001
M_m	27.55	.036193	.6126	-.0041	-.0006	.0001
M_f	13.66	.073002	.6109	-.0037	-.0006	.0001
75,565	13.63	.073149	.6109	-.0037	-.0006	.0001

Name	Period	Frequency	$l^{(0)R}$	$l^{(0)I}$	$l^{(1)}$	$l^{(2)}$	l'
Semidiurnal		-2	.0847	-.0007	.0024	.0002	
Diurnal							
Q_1	9.13	0.89080	.0846	-.0006	.0012	.0002	-.0002
145,545	13.63	0.92685	.0846	-.0006	.0012	.0002	-.0002
O_1	13.66	0.92700	.0846	-.0006	.0012	.0002	-.0002
No_1	27.55	0.96381	.0847	-.0006	.0012	.0002	-.0002
P_1	182.62	0.99454	.0853	-.0006	.0012	.0002	-.0002
165,545	6798.38	0.99985	.0869	-.0006	.0011	.0002	-.0003
K_1	infinity	1.00000	.0870	-.0006	.0011	.0002	-.0003
165,565	-6798.38	1.00015	.0872	-.0006	.0011	.0002	-.0003
ψ_1	-365.26	1.00273	.0710	-.0020	.0019	.0002	.0001
ϕ_1	-182.62	1.00546	.0828	-.0007	.0013	.0002	-.0002
J_1	-27.55	1.03619	.0845	-.0006	.0012	.0002	-.0002
Oo_1	-13.66	1.07300	.0846	-.0006	.0012	.0002	-.0002
Long period							
55,565	6798.38	.000147	.0936	-.0028	.0000	.0002	
S_{sa}	182.62	.005461	.0886	-.0016	.0000	.0002	
M_m	27.55	.036193	.0870	-.0012	.0000	.0002	
M_f	13.66	.073002	.0864	-.0011	.0000	.0002	
75,565	13.63	.073149	.0864	-.0011	.0000	.0002	

Step 1: Corrections to be computed in the time domain

in-phase	for degree 2 and 3	Nominal values
	. for degree 2 → eq (5)	$h_2 \to h(\phi) = h^{(0)} + h^{(2)}[(3\sin^2\phi - 1)/2]$
		$l_2 \to l(\phi) = l^{(0)} + l^{(2)}[(3\sin^2\phi - 1)/2]$
		$h^{(0)} = 0.6078$, $h^{(2)} = -0.0006$; $l^{(0)} = 0.0847$, $l^{(2)} = 0.0002$
	. for degree 3 → eq (6)	$h_3 = 0.292$ and $l_3 = 0.015$
out-of-phase	for degree 2 only	Nominal values
	. diurnal tides → eq (10)	$h^I = -0.0025$ and $l^I = -0.0007$
	. semidiurnal tides → eq (11)	$h^I = -0.0022$ and $l^I = -0.0007$
contribution	from latitude dependence	Nominal values
	. diurnal tides → eq (8)	$l^{(1)} = 0.0012$
	. semidiurnal tides → eq (9)	$l^{(1)} = 0.0024$

Step 2: Corrections to be computed in the frequency domain and to be added to the results of Step 1

in-phase	for degree 2	
	. diurnal tides → eqs (12)	→ Sum over all the components of Table 7.3a
	. semidiurnal tides	→ negligible
in-phase	and out-of-phase for degree 2	
	. long-period tides → eqs (13)	→ Sum over all the components of Table 7.3b

Displacement due to degree 2 tides, with nominal values for $h_{2m}^{(0)}$ and $l_{2m}^{(0)}$

The first stage of the Step 1 calculations employs real nominal values h_2 and l_2 common to all the degree 2 tides for the Love and Shida numbers. It is found to be computationally most economical to choose these to be the values for the semidiurnal tides (which have very little intra-band variation). On using the nominal values, the displacement vector of the station due to the degree 2 tides is given by

$$\Delta\vec{r} = \sum_{j=2}^{3} \frac{GM_j R_e^4}{GM_\oplus R_j^3} \left\{ h_2\ \hat{r} \left(\frac{3(\hat{R}_j \cdot \hat{r})^2 - 1}{2} \right) + 3l_2(\hat{R}_j \cdot \hat{r}) \left[\hat{R}_j - (\hat{R}_j \cdot \hat{r})\ \hat{r} \right] \right\}, \tag{5}$$

where $h_{22}^{(0)}$ and $l_{22}^{(0)}$ of the semidiurnal tides are chosen as the nominal values h_2 and l_2. The out-of-phase displacements due to the imaginary parts of the Love numbers are dealt with separately below. In Equation (5),

GM_j = gravitational parameter for the Moon ($j = 2$) or the Sun ($j = 3$),
$GM_\oplus$ = gravitational parameter for the Earth,
$\hat{R}_j, R_j$ = unit vector from the geocenter to Moon or Sun and the magnitude of that vector,
R_e = Earth's equatorial radius,
$\hat{r}, r$ = unit vector from the geocenter to the station and the magnitude of that vector,
h_2 = nominal degree 2 Love number,
l_2 = nominal degree 2 Shida number.

Note that the part proportional to h_2 gives the radial (not vertical) component of the tide-induced station displacement, and the terms in l_2 represent the vector displacement perpendicular to the radial direction (and not in the horizontal plane).

The computation just described may be generalized to include the latitude dependence arising through $h^{(2)}$ by simply adding $h^{(2)}\left[(3\sin^2\phi - 1)/2\right]$ to the constant nominal value given above, with $h^{(2)} = -0.0006$. The addition of a similar term (with $l^{(2)} = 0.0002$) to the nominal value of l_2 takes care of the corresponding contribution to the transverse displacement. The resulting incremental displacements are small, not exceeding 0.4 mm radially and 0.2 mm in the transverse direction.

Displacement due to degree 3 tides

The Love numbers of the degree 3 tides may be taken as real and constant in computations to the degree of accuracy aimed at here. The displacement vector due to these tides is then given by

$$\Delta\vec{r} = \sum_{j=2}^{3} \frac{GM_j R_e^5}{GM_\oplus R_j^4} \left\{ h_3\, \hat{r} \left(\frac{5}{2}(\hat{R}_j \cdot \hat{r})^3 - \frac{3}{2}(\hat{R}_j \cdot \hat{r}) \right) + l_3 \left(\frac{15}{2}(\hat{R}_j \cdot \hat{r})^2 - \frac{3}{2} \right) \left[\hat{R}_j - (\hat{R}_j \cdot \hat{r})\hat{r} \right] \right\}. \quad (6)$$

Only the Moon's contribution ($j = 2$) needs to be computed, the term due to the Sun being negligible. The transverse part of the displacement (6) does not exceed 0.2 mm, but the radial displacement can reach 1.7 mm.

Contributions to the transverse displacement due to the $l^{(1)}$ term

The imaginary part of $l^{(1)}$ is negligible, as is the intra-band variation of Re $l^{(1)}$; and $l^{(1)}$ is effectively zero in the zonal band.

In the expressions given below, and elsewhere in this chapter,

Φ_j = body fixed geocentric latitude of Moon or Sun, and
λ_j = body fixed east longitude (from Greenwich) of Moon or Sun.

The following formulae may be employed when the use of Cartesian coordinates X_j, Y_j, Z_j of the body relative to the terrestrial reference frame is preferred:

$$P_2^0(\sin\Phi_j) = \tfrac{1}{R_j^2}\left(\tfrac{3}{2}Z_j^2 - \tfrac{1}{2}R_j^2\right), \quad (7a)$$

$$P_2^1(\sin\Phi_j)\cos\lambda_j = \tfrac{3X_jZ_j}{R_j^2}, \qquad P_2^1(\sin\Phi_j)\sin\lambda_j = \tfrac{3Y_jZ_j}{R_j^2}, \quad (7b)$$

$$P_2^2(\sin\Phi_j)\cos 2\lambda_j = \tfrac{3}{R_j^2}(X_j^2 - Y_j^2), \qquad P_2^2(\sin\Phi_j)\sin 2\lambda_j = \tfrac{6}{R_j^2}X_jY_j. \quad (7c)$$

Contribution from the diurnal band (with $l^{(1)} = 0.0012$):

$$\delta\vec{t} = -l^{(1)}\sin\phi \sum_{j=2}^{3} \frac{GM_jR_e^4}{GM_\oplus R_j^3} P_2^1(\sin\Phi_j)\left[\sin\phi\cos(\lambda-\lambda_j)\ \hat{n} - \cos 2\phi\sin(\lambda-\lambda_j)\ \hat{e}\right]. \quad (8)$$

Contribution from the semidiurnal band (with $l^{(1)} = 0.0024$):

$$\delta\vec{t} = -\frac{1}{2}l^{(1)}\sin\phi\cos\phi \sum_{j=2}^{3} \frac{GM_jR_e^4}{GM_\oplus R_j^3} P_2^2(\sin\Phi_j)\left[\cos 2(\lambda-\lambda_j)\ \hat{n} + \sin\phi\sin 2(\lambda-\lambda_j)\ \hat{e}\right]. \quad (9)$$

The contributions of the $l^{(1)}$ term to the transverse displacement caused by the diurnal and semidiurnal tides could be up to 0.8 mm and 1.0 mm, respectively.

Out-of-phase contributions from the imaginary parts of $h_{2m}^{(0)}$ and $l_{2m}^{(0)}$

In the following, h^I and l^I stand for the imaginary parts of $h_{2m}^{(0)}$ and $l_{2m}^{(0)}$.

Contributions δr to radial and $\delta\vec{t}$ to transverse displacements from diurnal tides (with $h^I = -0.0025$, $l^I = -0.0007$):

$$\delta r = -\frac{3}{4}h^I \sum_{j=2}^{3} \frac{GM_jR_e^4}{GM_\oplus R_j^3} \sin 2\Phi_j \sin 2\phi \sin(\lambda-\lambda_j), \quad (10a)$$

$$\delta\vec{t} = -\frac{3}{2} l^I \sum_{j=2}^{3} \frac{GM_j R_e^4}{GM_\oplus R_j^3} \sin 2\Phi_j \left[\cos 2\phi \sin(\lambda - \lambda_j)\ \hat{n} + \sin\phi \cos(\lambda - \lambda_j)\ \hat{e}\right]. \tag{10b}$$

Contributions from semidiurnal tides (with h^I=−0.0022, l^I=−0.0007):

$$\delta r = -\frac{3}{4} h^I \sum_{j=2}^{3} \frac{GM_j R_e^4}{GM_\oplus R_j^3} \cos^2\Phi_j \cos^2\phi \sin 2(\lambda - \lambda_j), \tag{11a}$$

$$\delta\vec{t} = \frac{3}{4} l^I \sum_{j=2}^{3} \frac{GM_j R_e^4}{GM_\oplus R_j^3} \cos^2\Phi_j \left[\sin 2\phi \sin 2(\lambda - \lambda_j)\ \hat{n} - 2\cos\phi \cos 2(\lambda - \lambda_j)\ \hat{e}\right]. \tag{11b}$$

The out-of-phase contribution from the zonal tides has no closed expression in the time domain.

Computations of Step 2 take account of the intra-band variation of $h_{2m}^{(0)}$ and $l_{2m}^{(0)}$. Variations of the imaginary parts are negligible except as stated below (see Table 7.3a). For the zonal tides, however, the contributions from the imaginary part have to be computed in Step 2.

Correction for frequency dependence of the Love and Shida numbers

(a) Contributions from the diurnal band

Corrections, which include both in-phase (*ip*) and out-of-phase (*op*) parts, to the radial and transverse station displacements δr and $\delta\vec{t}$ due to a diurnal tidal term of frequency f are obtainable from Equation (1b):

$$\delta r = \left[\delta R_f^{(ip)} \sin(\theta_f + \lambda) + \delta R_f^{(op)} \cos(\theta_f + \lambda)\right] \sin 2\phi, \tag{12a}$$

$$\begin{aligned} \delta\vec{t} = & \left[\delta T_f^{(ip)} \cos(\theta_f + \lambda) - \delta T_f^{(op)} \sin(\theta_f + \lambda)\right] \sin\phi\ \hat{e} \\ + & \left[\delta T_f^{(ip)} \sin(\theta_f + \lambda) + \delta T_f^{(op)} \cos(\theta_f + \lambda)\right] \cos 2\phi\ \hat{n}, \end{aligned} \tag{12b}$$

where

$$\begin{aligned} \begin{pmatrix} \delta R_f^{(ip)} \\ \delta R_f^{(op)} \end{pmatrix} &= -\tfrac{3}{2}\sqrt{\tfrac{5}{24\pi}} H_f \begin{pmatrix} \delta h_f^R \\ \delta h_f^I \end{pmatrix}, \\ \begin{pmatrix} \delta T_f^{(ip)} \\ \delta T_f^{(op)} \end{pmatrix} &= -3\sqrt{\tfrac{5}{24\pi}} H_f \begin{pmatrix} \delta l_f^R \\ \delta l_f^I \end{pmatrix}, \end{aligned} \tag{12c}$$

and

δh_f^R and δh_f^I are the differences of $h^{(0)R}$ and $h^{(0)I}$ at frequency f from the nominal values h_2 and h^I used in Equations (5) and (10a), respectively,

δl_f^R and δl_f^I are the differences of $l^{(0)R}$ and $l^{(0)I}$ at frequency f from the nominal values l_2 and l^I used in Equations (5) and (10b), respectively.

(b) Contributions from the long-period band

Corrections δr and $\delta\vec{t}$ due to a zonal tidal term of frequency f include both *ip* and *op* parts. From Equations (1a) and (3) one finds

$$\delta r = \left(\frac{3}{2}\sin^2\phi - \frac{1}{2}\right) \left(\delta R_f^{(ip)} \cos\theta_f + \delta R_f^{(op)} \sin\theta_f\right), \tag{13a}$$

$$\delta\vec{t} = \left(\delta T_f^{(ip)} \cos\theta_f + \delta T_f^{(op)} \sin\theta_f\right) \sin 2\phi\ \hat{n}, \tag{13b}$$

Table 7.3a: Corrections due to the frequency dependence of Love and Shida numbers for diurnal tides. Units: mm. All terms with radial correction ≥ 0.05 mm are shown. Nominal values are $h_2 = 0.6078$ and $l_2 = 0.0847$ for the real parts, and $h^I = -0.0025$ and $l^I = -0.0007$ for the imaginary parts. Frequencies are given in degrees per hour.

Name	Frequency	Doodson	τ	s	h	p	N'	p_s	ℓ	ℓ'	F	D	Ω	$\Delta R_f^{(ip)}$	$\Delta R_f^{(op)}$	$\Delta T_f^{(ip)}$	$\Delta T_f^{(op)}$
Q_1	13.39866	135,655	1	-2	0	1	0	0	1	0	2	0	2	-0.08	0.00	-0.01	0.01
	13.94083	145,545	1	-1	0	0	-1	0	0	0	2	0	1	-0.10	0.00	0.00	0.00
O_1	13.94303	145,555	1	-1	0	0	0	0	0	0	2	0	2	-0.51	0.00	-0.02	0.03
No_1	14.49669	155,655	1	0	0	1	0	0	1	0	0	0	0	0.06	0.00	0.00	0.00
π_1	14.91787	162,556	1	1	-3	0	0	1	0	1	2	-2	2	-0.06	0.00	0.00	0.00
P_1	14.95893	163,555	1	1	-2	0	0	0	0	0	2	-2	2	-1.23	-0.07	0.06	0.01
	15.03886	165,545	1	1	0	0	-1	0	0	0	0	0	-1	-0.22	0.01	0.01	0.00
K_1	15.04107	165,555	1	1	0	0	0	0	0	0	0	0	0	12.00	-0.78	-0.67	-0.03
	15.04328	165,565	1	1	0	0	1	0	0	0	0	0	1	1.73	-0.12	-0.10	0.00
ψ_1	15.08214	166,554	1	1	1	0	0	-1	0	-1	0	0	0	-0.50	-0.01	0.03	0.00
ϕ_1	15.12321	167,555	1	1	2	0	0	0	0	0	-2	2	-2	-0.11	0.01	0.01	0.00

where

$$\begin{aligned} \begin{pmatrix} \delta R_f^{(ip)} \\ \delta R_f^{(op)} \end{pmatrix} &= \sqrt{\tfrac{5}{4\pi}} H_f \begin{pmatrix} \delta h_f^R \\ -\delta h_f^I \end{pmatrix}, \\ \begin{pmatrix} \delta T_f^{(ip)} \\ \delta T_f^{(op)} \end{pmatrix} &= \tfrac{3}{2}\sqrt{\tfrac{5}{4\pi}} H_f \begin{pmatrix} \delta l_f^R \\ -\delta l_f^I \end{pmatrix}. \end{aligned} \tag{13c}$$

Table 7.3b: Corrections due to the frequency dependence of Love and Shida numbers for zonal tides. Units: mm. All terms with radial correction ≥ 0.05 mm are shown. Nominal values are $h = 0.6078$ and $l = 0.0847$. Frequencies are given in degrees per hour.

Name	Frequency	Doodson	τ	s	h	p	N'	p_s	ℓ	ℓ'	F	D	Ω	$\Delta R_f^{(ip)}$	$\Delta R_f^{(op)}$	$\Delta T_f^{(ip)}$	$\Delta T_f^{(op)}$
	0.00221	55,565	0	0	0	0	1	0	0	0	0	0	1	0.47	0.16	0.23	0.07
S_{sa}	0.08214	57,555	0	0	2	0	0	0	0	0	-2	2	-2	-0.20	-0.11	-0.12	-0.05
M_m	0.54438	65,455	0	1	0	-1	0	0	-1	0	0	0	0	-0.11	-0.09	-0.08	-0.04
M_f	1.09804	75,555	0	2	0	0	0	0	0	0	-2	0	-2	-0.13	-0.15	-0.11	-0.07
	1.10024	75,565	0	2	0	0	1	0	0	0	-2	0	-1	-0.05	-0.06	-0.05	-0.03

Values of ΔR_f and ΔT_f listed in Table 7.3a and 7.3b are for the constituents that must be taken into account to ensure an accuracy of 1 mm.

A Fortran program for computing the Steps 1 and 2 corrections is available at <[1]>.

7.1.1.2 *Permanent deformation*

The tidal model described above in principle contains a time-independent part so that the coordinates obtained by taking into account this model in the analysis will be "conventional tide free" values. (Note that they do *not* correspond to what would be observed in the absence of tidal perturbation. See the discussion in Chapter 1.) This section allows a user to compute "mean tide" coordinates from "conventional tide free" coordinates.

Specifically, the degree 2 zonal tide generating potential includes a spectral component of zero frequency and amplitude $H_0 = -0.31460$ m, and its effect enters the tidal displacement model

[1] `ftp://tai.bipm.org/iers/conv2010/chapter7/dehanttideinel.f`

through the time-independent component of expression (5). Evaluation of this component may be done using Equations (1a) and (2) with $H_f = H_0, \theta_f = 0$, and with the same nominal values for the Love number parameters as were used in Step 1: $h_2 = 0.6078, l_2 = 0.0847$ along with $h^{(2)} = -0.0006$ and $l^{(2)} = 0.0002$. One finds the radial component of the permanent displacement according to (5) to be

$$[-0.1206 + 0.0001 P_2(\sin\phi)]\, P_2(\sin\phi) \tag{14a}$$

in meters, and the transverse component to be

$$[-0.0252 - 0.0001 P_2(\sin\phi)] \sin 2\phi \tag{14b}$$

in meters northwards, where $P_2(\sin\phi) = (3\sin^2\phi - 1)/2$.

These are the components of the vector to be added to the "conventional tide free" computed tide-corrected position to obtain the "mean tide" position. The radial component of this restitution to obtain the "mean tide" value amounts to about −12 cm at the poles and about +6 cm at the equator.

7.1.2 Local site displacement due to ocean loading

Ocean tides cause a temporal variation of the ocean mass distribution and the associated load on the crust and produce time-varying deformations of the Earth that can reach 100 mm. The modeling of the associated site displacement is dealt with in this section.

Note on motion of the center of mass of the solid Earth

When the solid Earth together with the fluid masses are considered as a system without any external forces acting upon it, the position of the common center of mass remains fixed in space. When a phenomenon, such as the ocean tides, causes displacements of fluid masses, the center of mass of the fluid masses moves periodically and must be compensated by an opposite motion of the center of mass of the solid Earth. The stations, being fixed to the solid Earth, are subject to this counter-motion.

For observing techniques that rely upon the dynamical motion of satellites, which respond to the center of mass of the total Earth system, the modeled motions of crust-fixed stations should include the "geocenter motion" contributions that counterbalance the effects of the fluid components. For other observing techniques, such as VLBI, neglect of geocenter motion should have no observable consequences.

Models for ocean tidal loading

The tide generating potential due to the gravitational attraction of the Moon and the Sun can be described by an expansion into a set of tidal harmonics (*e.g.* Hartmann and Wenzel, 1995; Tamura, 1987; Cartwright and Tayler, 1971; Cartwright and Edden, 1973). The response of the oceans, unlike for the solid Earth, is strongly dependent on local and regional conditions that affect fluid flow. Closed-form analytical expressions are not adequate to describe the ocean tidal response globally. Instead, gridded formulations are needed. Table 7.4 lists the leading global ocean tidal models that have been developed since Schwiderski and Szeto (1981). Most modern models assimilate sea surface height measurements made by altimetry satellites.

The crustal loading at a particular location due to a given tidal harmonic is computed by integrating the tide height with a weighting function (Green's function, see Farrell, 1972), carrying the integration over all the ocean masses. The total loading may be obtained by summing the effect of all harmonics. In practice, the three-dimensional site displacements due to ocean tidal loading are computed using the following scheme. Let Δc denote a displacement component (radial, west, south) at a particular site at time t. Δc is obtained as

$$\Delta c = \sum_j A_{cj} \cos(\chi_j(t) - \phi_{cj}), \tag{15}$$

where the summation is carried out for a set of tidal constituents. The amplitudes A_{cj} and phases ϕ_{cj} describe the loading response for the chosen site. The astronomical argument $\chi_j(t)$ for the 11 main tides can be computed with the subroutine ARG2.F, which can be obtained at <[2]>.

Conventionally, only a discrete set of harmonics in the long-period (order $m = 0$), diurnal ($m = 1$) and semidiurnal ($m = 2$) bands are usually considered explicitly. The 11 main tides considered are the semidiurnal waves M_2, S_2, N_2, K_2, the diurnal waves K_1, O_1, P_1, Q_1, and the long-period waves M_f, M_m, and S_{sa}. The site-dependent amplitudes A_{cj} and phases ϕ_{cj} for these 11 tides are obtained as described in the next sub-section. Amplitudes and phases for other tidal constituents can be obtained from those of the 11 main tides by a variety of approximation schemes. For instance, if one wishes to include the effect of sidelobes of the main tides generated by modulation with the 18.6-year lunar node, then suitable adjustments in the 11 amplitudes and phases can be applied so that

$$\Delta c = \sum_{k=1}^{11} f_k A_{ck} \cos(\chi_k(t) + u_k - \phi_{ck}), \tag{16}$$

where f_k and u_k depend on the longitude of the lunar node. See Scherneck (1999) for the expression of these arguments.

In more complete methods, the lesser tides are handled by interpolation of the admittances using some full tidal potential development (*e.g.* Hartmann and Wenzel, 1995). One of these methods has been chosen as the conventional IERS method, and has been implemented in a subroutine that is recommended as a conventional computation of the loading displacement (see sub-section "Conventional routine to compute the ocean loading displacement" below).

Note that complete neglect of the minor tides and nodal modulations, using (15) with only the 11 main tides, is not recommended and may lead to errors of several mm, up to 5 mm rms at high latitudes (Hugentobler, 2006).

Additional contributions to ocean-induced displacement arise from the frequency dependence of the load Love numbers due to the Nearly Diurnal Free Wobble in the diurnal tidal band. The effect of this dependence has been taken into account, following Wahr and Sasao (1981), by incrementing the *body tide* Love numbers as explained in Section 7.1.1.

Site-dependent tidal coefficients

For a given site, the amplitudes A_{cj} and phases $\phi_{cj}, 1 \leq j \leq 11$, for the 11 main tides may be obtained electronically from the ocean loading service site at <[3]>; see Scherneck (1991). They are provided in either the so-called BLQ format or in the HARPOS format. An example for the BLQ format is given in Table 7.5. Note that tangential displacements are to be taken positive in west and south directions. The service allows coefficients to be computed selectably from any of eighteen ocean tide models; see Table 7.4.

The accuracy of the ocean tide loading values depends on the errors in the ocean tide models, the errors in the Green's function, the coastline representation and the numerical scheme of the loading computation itself. To have a correct representation of the water areas one normally uses a high resolution coastline of around 600 m to 2 km. Note that still some problems exist near Antarctica where one should use the real land coastline instead of the ice shelve edges. Different elastic Earth models produce different Green's functions but their differences are small, less than 2%. Most numerical schemes to compute the loading are good to about 2-5%. Currently, the largest contributor to the uncertainty in the loading value are the errors in the ocean tide models. Therefore it is recommended to use the most recent ocean tide models (TPXO7.2, see <[4]> for a solution derived using tide gauge and TOPEX/Poseidon data; FES2004 for a hydrodynamic solution with altimetry data). However, older models might sometimes be preferred for internal consistency. Since many space geodesy stations are inland or near coasts, the accuracy of the tide

[2] `ftp://tai.bipm.org/iers/conv2010/chapter7`
[3] `http://froste.oso.chalmers.se/loading`
[4] `http://volkov.oce.orst.edu/tides/TPXO7.2.html`

models in the shelf areas is more crucial than in the open sea. Load convolution adopts land-sea masking according to the high resolution coastlines dataset included in the Generic Mapping Tools (GMT, Wessel and Smith, 1998). Ocean tide mass budgets have been constrained using a uniform co-oscillation oceanic layer. The integrating loading kernel employs a disk-generating Green's function method (Farrell, 1972; Zschau, 1983; Scherneck, 1990).

When generating tables of amplitudes and phases using the ocean loading service, one has to answer the question "Do you want to correct your loading values for the [geocenter] motion?"

Answering "No" means that the coefficients do not include the large-scale effect of the geocenter motion caused by the ocean tide. This is appropriate for station coordinates given in a "crust-fixed" frame that is not sensitive to the Earth's center of mass.

Answering "Yes" means that the coefficients include the large-scale effect of the geocenter motion caused by the ocean tide. This is consistent with data analyses that realize a near-instantaneous "center of mass" frame using observations of satellite dynamics.

Table 7.4: Ocean tide models available at the automatic loading service.

Model code	Reference	Input	Resolution
Schwiderski	Schwiderski (1980)	Tide gauge	$1° \times 1°$
CSR3.0, CSR4.0	Eanes (1994)	TOPEX/Poseidon altim.	$1° \times 1°$
	Eanes and Bettadpur (1995)	T/P + Le Provost loading	$0.5° \times 0.5°$
TPXO5	Egbert *et al.* (1994)	inverse hydrodyn. solution from T/P altim.	256×512
TPXO6.2	Egbert *et al.* (2002), see <[4]>	idem	$0.25° \times 0.25°$
TPXO7.0, TPXO7.1	idem	idem	idem
FES94.1	Le Provost *et al.* (1994)	numerical model	$0.5° \times 0.5°$
FES95.2	Le Provost *et al.* (1998)	num. model + assim. altim.	$0.5° \times 0.5°$
FES98	Lefèvre *et al.* (2000)	num. model + assim. tide gauges	$0.25° \times 0.25°$
FES99	Lefèvre *et al.* (2002)	numerical model + assim. tide gauges and altim.	$0.25° \times 0.25°$
FES2004	Letellier (2004)	numerical model	$0.125° \times 0.125°$
GOT99.2b, GOT00.2	Ray (1999)	T/P	$0.5° \times 0.5°$
GOT4.7	idem	idem	idem
EOT08a	Savcenko *et al.* (2008)	Multi-mission altimetry	$0.125° \times 0.125°$
AG06a	Andersen (2006)	Multi-mission altimetry	$0.5° \times 0.5°$
NAO.99b	Matsumoto *et al.* (2000)	num. + T/P assim.	$0.5° \times 0.5°$

Conventional routine to compute the ocean loading displacement

D. Agnew has provided a Fortran program (HARDISP.F) to compute the ocean tide loading displacements for a site, given the amplitudes A_{cj} and phases $\phi_{cj}, 1 \leq j \leq 11$, as generated by the Bos-Scherneck website (in BLQ format, see above). The implementation considers a total of 342 constituent tides whose amplitudes and phases are found by spline interpolation of the tidal admittances based on the 11 main tides. Tests have been carried out showing that differences with an earlier version of HARDISP.F with 141 constituent tides are of order 0.1 mm rms. Comparisons with the ETERNA software of Wenzel (1996) have been carried out by M. Bos (2005), who concludes that the routine is precise to about 1%. Uncertainties in the ocean models are generally larger. The code for the routine can be obtained at <[2]>.

Center of mass correction

If necessary, the crust-frame translation (geocenter motion) due to the ocean tidal mass, $dX(t)$, $dY(t)$, and $dZ(t)$, may be computed according to the method given by Scherneck at <[5]>, *e.g.* for $dX(t)$ as

[5] `http://froste.oso.chalmers.se/loading/cmc.html`

Table 7.5: Sample of an ocean loading table file in BLQ format. Each site record shows a header with information on the ocean tide model and the site name and geographic coordinates. First three rows of numbers designate amplitudes (meter), radial, west, south, followed by three lines with the corresponding phase values (degrees).

Columns designate partial tides $M_2, S_2, N_2, K_2, K_1, O_1, P_1, Q_1, M_f, M_m$, and S_{sa}.

```
$$
  ONSALA
$$ CSR4.0_f_PP ID: 2009-06-25 20:02:03
$$ Computed by OLMPP by H G Scherneck, Onsala Space Observatory, 2009
$$ Onsala,                                  lon/lat: 11.9264      57.3958
.00352   .00123   .00080   .00032   .00187   .00112   .00063   .00003   .00082   .00044   .00037
.00144   .00035   .00035   .00008   .00053   .00049   .00018   .00009   .00012   .00005   .00006
.00086   .00023   .00023   .00006   .00029   .00028   .00010   .00007   .00004   .00002   .00001
   -64.7     -52.0     -96.2     -55.2     -58.8    -151.4     -65.6    -138.1       8.4       5.2       2.1
    85.5     114.5      56.5     113.6      99.4      19.1      94.1     -10.4    -167.4    -170.0    -177.7
   109.5     147.0      92.7     148.8      50.5     -55.1      36.4    -170.4     -15.0       2.3       5.2
```

$$dX(t) = \sum_{k=1}^{11} X_{in}(k)\cos(\chi_k(t)) + X_{cr}(k)\sin(\chi_k(t)) \tag{17}$$

where the in-phase ($_{in}$) and cross-phase ($_{cr}$) amplitudes (in meters) are tabulated for the various ocean models. Similarly for $dY(t)$ and $dZ(t)$. This correction should be applied, for instance, in the transformation of GPS orbits from the center-of-mass to the crust-fixed frame expected in the sp3 orbit format

$$X_{crust-fixed} = X_{center-of-mass} - dX, \tag{18}$$

i.e. the translation vector should be substracted when going from center-of-mass to sp3.

7.1.3 S_1-S_2 atmospheric pressure loading

The diurnal heating of the atmosphere causes surface pressure oscillations at diurnal S_1, semidiurnal S_2, and higher harmonics. These "atmospheric tides" induce periodic motions of the Earth's surface (Petrov and Boy, 2004). Previously, the S_1 and S_2 loading effects have not been included in the station motion model. Figure 7.1 shows the amplitude and phase of the predicted vertical deformation of the S_1 and S_2 tides derived from the model of Ray and Ponte (2003) using elastic Green's functions (Farrell, 1972) in the center of mass of Earth + fluid masses (CM) frame. Horizontal deformations (not shown) are a factor of 10 smaller in amplitude. The amplitude of the vertical deformation is equal to that of some ocean tide loading effects and should, therefore, be considered in the station motion model. Being close to the orbital period of the GPS satellites, modeling of the S_2 effect is especially important for this technique in order to minimize aliasing (Tregoning and Watson, 2009).

The conventional recommendation is to calculate the station displacement using the Ray and Ponte (2003) S_2 and S_1 tidal model, hereafter referred to as RP03.

Tidal model

The S_1 and S_2 RP03 tidal model is derived from the European Centre for Medium-Range Weather Forecasts (ECMWF) operational global surface pressure fields, using a procedure outlined by van den Dool *et al.* (1997). The S_2 model has been tested by comparison against 428 barometer

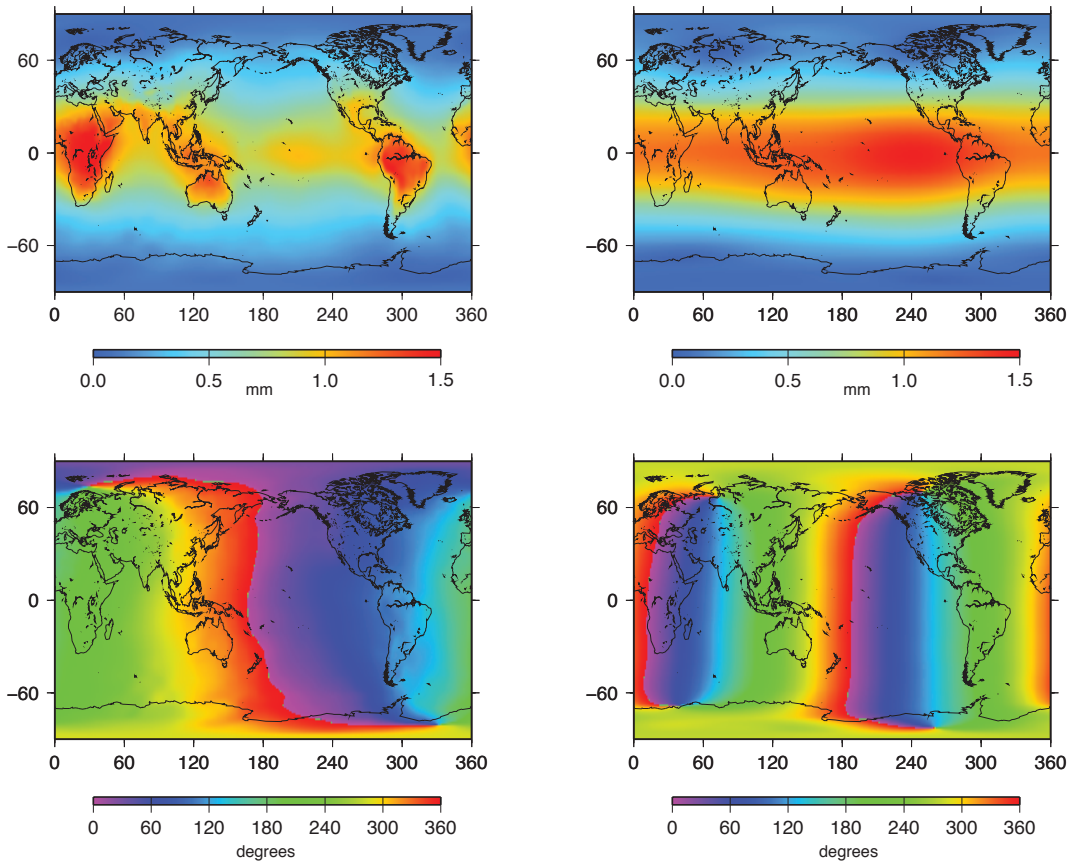

Figure 7.1: Amplitude (in mm) and phase (in degrees) of the predicted vertical surface displacement from the S_1 and S_2 atmospheric tides from the model by Ray and Ponte (2003).

stations (Ray and Ponte, 2003). It is expected that National Centers for Environmental Prediction (NCEP) operational data provide equivalent results (van den Dool, 2004). Similar comparisons were found for the S_1 models, although those tests were far less extensive. The barometer stations have also revealed small phase errors in the derived tidal fields. The origin of these errors is not understood, but the models can be corrected *a posteriori*. The RP03 phases have been adjusted by 20 minutes to correct for this error.

Calculation of loading effects

We use elastic Green's functions (Farrell, 1972) derived in the various reference frames to generate the predicted in-phase and out-of-phase surface displacement from RP03. The spatial resolution of the input surface pressure grid is 1.125°.

Elastic Green's functions (versus frequency-dependent Green's functions) are sufficient for this computation. By considering changes in viscoelasticity, Francis and Mazzega (1990) demonstrated that the amplitude of the M_2 ocean tidal radial surface displacement can vary by 1.5% and the

phase by 3%, *i.e.* a negligible amount in comparison to uncertainties in the ocean tide model itself. A 1.5% effect on the S_2 radial displacement is 0.05 mm in amplitude which is certainly less than the uncertainty in the S_1 and S_2 pressure models and can be ignored.

In addition, differences in predicted displacements derived from different Green's functions are on the order of 0.1 mm rms, so it seems unnecessary to generate corrections using Green's functions derived for different Earth models. The three-dimensional surface displacements are determined by assuming that the oceans respond as the solid Earth to the load, *i.e. no* inverted barometer. At these frequencies, the ocean does not have time to achieve equilibrium. Furthermore, it should be noted that the ocean's response to these atmospheric tides is already modeled separately through the site displacements due to ocean tidal loading described in Section 7.1.1.

The phase convention follows that of RP03. At any geographic location, at any time, the tidal deformation, expressed in terms of up, east and north components, is the sum of $d(u,e,n)_{S_1}$ and $d(u,e,n)_{S_2}$ defined as

$$d(u,e,n)_{S_1} = A_{d1}(u,e,n) * cos(\omega_1 T) + B_{d1}(u,e,n) * sin(\omega_1 T) \tag{19a}$$

$$d(u,e,n)_{S_2} = A_{d2}(u,e,n) * cos(\omega_2 T) + B_{d2}(u,e,n) * sin(\omega_2 T), \tag{19b}$$

where $A_{d1}, B_{d1}, A_{d2}, B_{d2}$ are the surface displacement coefficients expressed in the same length unit as the deformation components, T is UT1 in days and ω_1 and ω_2 are the frequencies of the S_1 and S_2 atmospheric tides, *e.g.* $\omega_1 = 1$ cycle/day and $\omega_2 = 2$ cycles/day.

The surface displacement coefficients $A_{d1}, B_{d1}, A_{d2}, B_{d2}$ are determined for each site by performing a global convolution sum of the Green's functions with the $cos_{S_1}, sin_{S_1}, cos_{S_2}, sin_{S_2}$ pressure mass coefficients. Gridded values of the three-dimensional predicted surface displacements from the RP03 model may be found at <[6]>. Corrections for the vertical surface displacement are usually sufficient, whereas estimates of horizontal effects are provided for completeness. The grids are provided for the two fundamental reference frames used for geodetic data analysis: center of solid Earth (CE) and center of mass of Earth + atmosphere + ocean + water storage (CM). In most applications, *e.g.* corrections of satellite-based techniques at the observation level, the CM frame is most appropriate. A description of the grid indexing as well as a program `grdintrp.f` for interpolating the grids are also available at <[6]>.

Center of mass correction

As with ocean tidal loading (see preceding section), it may be necessary to compute the crust-frame translation (geocenter motion) due to the atmospheric tidal mass. $dX(t)$, $dY(t)$, and $dZ(t)$ may be computed according to the method given by Scherneck at <[7]>, *e.g.* for $dX(t)$ as

$$dX(t) = A_1 cos(\omega_1 T) + B_1 sin(\omega_1 T) + A_2 cos(\omega_2 T) + B_2 sin(\omega_2 T) \tag{20}$$

where, as above, $\omega_1 = 1$ cycle/day and $\omega_2 = 2$ cycles/day and A_1, B_1, A_2, B_2 are the amplitudes of the in-phase and out-of-phase components of the atmospheric tides (in meters) and are given in Table 7.6 and in the file `com.dat` available at <[6]>. As with ocean tidal loading (see preceding section), this correction should be applied in transforming GPS orbits from the center-of-mass to the crust-fixed frame expected in the sp3 orbit format.

Table 7.6: Coefficients for the center of mass correction of the S_1-S_2 atmospheric pressure loading

	A_1	B_1	A_2	B_2
dX	2.1188E-04	-7.6861E-04	1.4472E-04	-1.7844E-04
dY	-7.2766E-04	-2.3582E-04	-3.2691E-04	-1.5878E-04
dZ	-1.2176E-05	3.2243E-05	-9.6271E-05	1.6976E-05

[6] `http://geophy.uni.lu/ggfc-atmosphere/tide-loading-calculator.html`
[7] `http://froste.oso.chalmers.se/loading/cmc.html`

7.1.4 Rotational deformation due to polar motion

Changes in the direction of the Earth's rotation axis with respect to a location on the Earth's surface cause changes in the gravitational potential (Agnew, 2007) that translate into local deformations (Desai, 2002). This pole tide may cause variations in station coordinates of the order of a few centimeters. In a terrestrial reference system with the $\hat{z}$-axis oriented along the mean rotation axis of the Earth, the $\hat{x}$-axis directed toward the adopted origin of longitude, and the $\hat{y}$-axis in the
2015/06/19 plane of the 90° E meridian and orthogonal to the $\hat{x}$ and $\hat{z}$-axis, the centrifugal potential caused by the Earth's rotation at a point on the Earth's surface is given by

$$V = \frac{1}{2}\left[|\vec{r}|^2|\vec{\Omega}|^2 - (\vec{r}\cdot\vec{\Omega})^2\right], \tag{21}$$

where $\vec{\Omega} = |\vec{\Omega}|\,[m_1\ \hat{x} + m_2\ \hat{y} + (1+m_3)\hat{z}]$. $|\vec{\Omega}\ |$is the mean angular speed of the Earth's rotation; m_1, m_2 describe the time-dependent offset of the instantaneous rotation pole from the mean, and m_3, the fractional variation in the rotation rate, and $\vec{r}$ is the geocentric vector directed toward the site. Neglecting the variations in m_3 which induce displacements that are below the millimeter level, the m_1 and m_2 terms produce a perturbation in the potential V at a site with longitude λ and co-latitude θ (Wahr, 1985):

$$\Delta V(r,\theta,\lambda) = -\frac{|\vec{\Omega}|^2|\vec{r}|^2}{2}\sin 2\theta\,(m_1\cos\lambda + m_2\sin\lambda). \tag{22}$$

where θ is the colatitude of the station. The radial displacement S_r and the horizontal displacements S_θ and S_λ (positive upwards, south and east respectively in a horizon system at the station) due to ΔV are obtained using the formulation of tidal Love numbers h_2 and ℓ_2 (Munk and MacDonald, 1960):

$$S_r = h_2\frac{\Delta V}{g}, \qquad S_\theta = \frac{\ell_2}{g}\partial_\theta\Delta V, \qquad S_\lambda = \frac{\ell_2}{g}\frac{1}{\sin\theta}\partial_\lambda\Delta V. \tag{23}$$

The variables m_1 and m_2 can be derived from the polar motion variables (x_p, y_p) defined in Chapter 5:

$$m_1 = x_p - \bar{x}_p, \qquad m_2 = -(y_p - \bar{y}_p). \tag{24}$$

where $\bar{x}_p$ and $\bar{y}_p$ are the time varying angular coordinates of the mean rotational pole in the terrestrial reference frame, referred to as the mean pole.The mean pole is defined by the coordinates of a pole that is free of the principal periodic motions of the rotational pole, *i.e.* the Chandler and annual motions, as well as other high-frequency motions. In practice, the coordinates of $\bar{x}_p$ and $\bar{y}_p$ are determined by filtering the observed time series, $x_p(t)$ and $y_p(t)$ to remove variations with characteristic frequencies greater than 0.05 yr^{-1}. To ensure that the geopotential field is aligned to the mean pole (see Section 6.1) within the present geodetic accuracy, estimates of the mean pole
2015/06/19 coordinates accurate to ± 10 milli-arcseconds should be used.

For this purpose, a Conventional Mean Pole (CMP) model is provided by the IERS Conventions. The CMP was provided previously in the IERS Conventions (2003) as a linear model and in the IERS Conventions (2010) as a cubic model with a linear extrapolation after 2010.0. However, in view of present-day ice sheet mass losses, the motion of the mean pole is not likely to be predictable (see *e.g.*, Chen, *et al.* 2013) at the level required for the pole tide correction. Therefore, starting with year 2015, the CMP of the IERS Conventions will no longer be represented by a polynomial but will be provided by a FORTRAN subroutine, updated yearly and referenced as IERS_CMP_YYYY.f for year YYYY, based on observations made available by the IERS Earth Orientation Centre. At the beginning of year YYYY, the IERS Earth Orientation Centre will generate a table of observed values of the mean pole with the last point at epoch YYYY.0 by filtering periodic terms in the
2015/06/19 EOP(IERS) C01 series <[8]>.

[8] `ftp://hpiers.obspm.fr/iers/eop/eopc01`

The IERS Convention Center then incorporates it in the subroutine IERS_CMP_YYYY.f, updated annually at <[9]>, that generates the components $\bar{x}_p$ and $\bar{y}_p$ of the IERS CMP(YYYY) for epochs after 1970.

These values are computed by linear interpolation of the yearly values taken from the observations provided by the IERS Earth Orientation Centre. Because of the filtering process, the values of the mean pole are likely to change as the polar motion time series is extended, but the changes should remain within the range of the required accuracy. The subroutine also provides options to obtain the CMP coordinates as described in previous versions of the IERS Conventions. The use of the most recent version is recommended as significant departures from observations may result using earlier versions for years that lie outside of the range for which they were designed. In any case, users should document the version they use. 2015/06/19

It is noted that the current model is intended to remove the effects of rotational deformation at the annual and Chandler periods. However, it may be that the model is deficient with respect to longer-term variations, particularly in light of the recent polar ice-sheet mass losses that have changed the path of the mean pole considerably. For example, King and Watson (2014) suggest the adoption of a linear mean pole based on the "timescale of interest" in order to capture the variations about that long-term rate as part of the rotational deformation model. However, at this time, the best model for the mean pole model remains an open question. 2015/06/19

Using Love number values appropriate to the frequency of the pole tide ($h_2 = 0.6207$, $\ell_2 = 0.0836$) and $|\vec{r}| = a = 6.378 \times 10^6$ m, the displacements in millimeters are

$$\begin{aligned} S_\theta &= -9\cos 2\theta\,(m_1 \cos\lambda + m_2 \sin\lambda) \text{ in mm,} \\ S_\lambda &= 9\cos\theta\,(m_1 \sin\lambda - m_2 \cos\lambda) \text{ in mm,} \\ S_r &= -33\sin 2\theta\,(m_1 \cos\lambda + m_2 \sin\lambda) \text{ in mm,} \end{aligned} \tag{25}$$

with m_1 and m_2 given in arcseconds. Note that the values of the Love numbers include the anelastic contributions to the real part, which induce a contribution to the displacement of order 1 mm, but do not include the contributions to the imaginary part, whose effects are about 5 times smaller. Taking into account that m_1 and m_2 vary, at most, by 0.8 arcseconds, the maximum radial displacement is approximately 25 mm, and the maximum horizontal displacement is about 7 mm. If X, Y, and Z are Cartesian coordinates of a station in a right-handed equatorial coordinate system, the changes in them due to the pole tide are

$$[dX, dY, dZ]^T = R^T [S_\theta, S_\lambda, S_r]^T, \tag{26}$$

where

$$R = \begin{pmatrix} \cos\theta\cos\lambda & \cos\theta\sin\lambda & -\sin\theta \\ -\sin\lambda & \cos\lambda & 0 \\ \sin\theta\cos\lambda & \sin\theta\sin\lambda & \cos\theta \end{pmatrix}. \tag{27}$$

7.1.5 Ocean pole tide loading

The ocean pole tide is generated by the centrifugal effect of polar motion on the oceans. This centrifugal effect is defined in equation (22) of Section 6.4. Polar motion is dominated by the 14-month Chandler wobble and annual variations. At these long periods, the ocean pole tide is expected to have an equilibrium response, where the displaced ocean surface is in equilibrium with the forcing equipotential surface. 2015/06/19

Desai (2002) presents a self-consistent equilibrium model of the ocean pole tide. This model accounts for continental boundaries, mass conservation over the oceans, self-gravitation, and loading of the ocean floor. Using this model, the load of the ocean pole tide produces the following deformation vector at any point on the surface of the Earth with latitude ϕ and longitude λ. The load

[9] `ftp://tai.bipm.org/iers/convupdt/chapter7/`

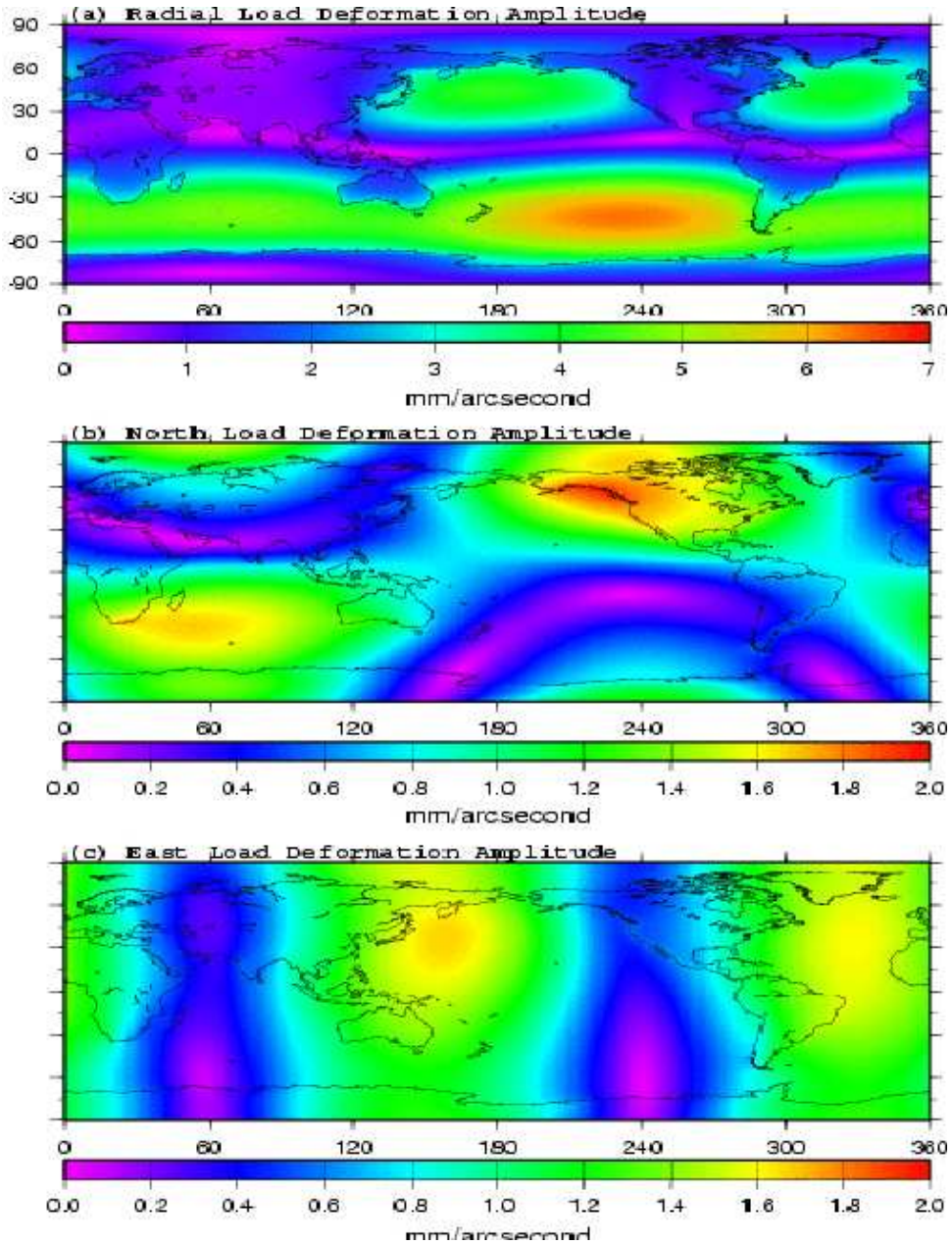

Figure 7.2: Loading from ocean pole tide: Amplitude as a function of the amplitude of wobble variable.

deformation vector is expressed here in terms of radial, north and east components, u_r, u_n, and u_e, respectively, and is a function of the wobble parameters (m_1, m_2).

$$\begin{bmatrix} u_r(\phi,\lambda) \\ u_n(\phi,\lambda) \\ u_e(\phi,\lambda) \end{bmatrix} = K \left\{ (m_1\gamma_2^R + m_2\gamma_2^I) \begin{bmatrix} u_r^R(\phi,\lambda) \\ u_n^R(\phi,\lambda) \\ u_e^R(\phi,\lambda) \end{bmatrix} + (m_2\gamma_2^R - m_1\gamma_2^I) \begin{bmatrix} u_r^I(\phi,\lambda) \\ u_n^I(\phi,\lambda) \\ u_e^I(\phi,\lambda) \end{bmatrix} \right\} \quad (28)$$

where

$$K = \frac{4\pi G a_E \rho_w H_p}{3 g_e}$$

$$H_p = \left(\frac{8\pi}{15}\right)^{1/2} \frac{\Omega^2 a_E^4}{GM}$$

and
Ω, a_E, GM, g_e, and G are defined in Chapter 1,
ρ_w = density of sea water = 1025 kg m^{-3},
$\gamma = (1 + k_2 - h_2) = \gamma_2^R + i\gamma_2^I = 0.6870 + 0.0036i$ (Values of k_2 and h_2 appropriate for the pole tide are as given in Sections 6.2 and 7.1.4),
(m_1, m_2) are the wobble parameters. Refer to Section 7.1.4 for the relationship between the wobble variables (m_1, m_2) and the polar motion variables (x_p, y_p).
$u_r^R(\phi,\lambda)$, $u_n^R(\phi,\lambda)$, $u_e^R(\phi,\lambda)$ are the real part of the ocean pole load tide coefficients.
$u_r^I(\phi,\lambda)$, $u_n^I(\phi,\lambda)$, $u_e^I(\phi,\lambda)$ are the imaginary part of the ocean pole load tide coefficients.

Maps of the required ocean pole load tide coefficients are available on an equally spaced 0.5 by 0.5 degree global grid at <[10]>. These coefficients provide the surface deformations with respect to the instantaneous center of mass of the deformed Earth including the mass of the loading ocean pole tide. Note that in (28) pole load tide coefficients are dimensionless so that the load deformation vector is expressed in the same length unit as K if the wobble parameters are expressed in rd. 2015/06/19

The amplitude of this loading deformation is shown in Figure 7.2 in mm per arcsecond as a function of the amplitude m of the wobble components (m_1, m_2). Given that the amplitude of the wobble variable is typically of order 0.3 arcseconds, the load deformation is typically no larger than about (1.8, 0.5, 0.5) mm in (radial, north, east) component, but it may occasionally be larger.

7.2 Models for other non-conventional displacement of reference markers on the crust

It is envisioned that this section describes methods of modeling non-tidal displacements associated with changing environmental loads, *e.g.* from atmosphere, ocean and hydrology. For this purpose, models should be made available to the user community through the IERS Global Geophysical Fluid Center and its special bureaux, together with all necessary supporting information, implementation documentation, and software.

At the time of this registered edition of the *IERS Conventions*, it is recommended not to include such modeling in operational solutions that support products and services of the IERS. Nevertheless, the non-tidal loading effects can be considered in other studies, and this section will be updated as adopted models become available.

7.3 Models for the displacement of reference points of instruments

This section lists effects which are to be considered when relating the reference point of an instrument used in a given technique to a marker that may be used as a reference by other techniques. Typical examples are antenna phase center offsets. These effects are technique-dependent and the conventional models for these effects are kept and updated by the technique services participating to the IERS: The IVS <[11]> for very long baseline interferometry, the ILRS <[12]> for satellite laser

[10] `ftp://tai.bipm.org/iers/conv2010/chapter7/opoleloadcoefcmcor.txt.gz`
[11] `http://ivscc.gsfc.nasa.gov/`
[12] `http://ilrs.gsfc.nasa.gov/`

ranging, the IGS <[13]> for global navigation satellite systems and the IDS <[14]> for DORIS. This section provides a short description of these models and directs the user to the original source of information.

7.3.1 Models common to several techniques

As some of the effects depend on local environmental conditions, conventional models for these effects need to be based on a reference value for local temperature. A conventional model to determine reference temperature is given below.

Reference temperature

If necessary, it is recommended to determine the reference temperature values with the model GPT (Boehm *et al.*, 2007) which is based on a spherical harmonic expansion of degree and order 9 with an annual periodicity, and is provided as a Fortran routine, `GPT.F`, at <[15]> and <[16]>. The arguments of the routine are described in its header. The model assumes a yearly signature and no secular variation, so should not impact secular terms in the modeled geodetic data. If only a constant reference temperature is needed (no yearly term), the model value at the 119th day of year, 07:30 UTC (e.g. MJD 44357.3125) should be used.

7.3.2 Very long baseline interferometry

Thermal expansion

VLBI antennas are subject to structural deformations due to temperature variations that can cause variations in the VLBI delay exceeding 10 ps. Correspondingly, the coordinates of the reference point may vary by several mm. For this reason the IVS has developed a model for VLBI antenna thermal deformation (Nothnagel, 2008) that is to be used in its routine product generation. The conventional model for VLBI antenna thermal deformation may be found at <[17]>.

7.3.3 Global navigation satellite systems

Antenna phase center offsets and variations

The exact phase center position of the transmitting as well as of the receiving antenna depends on the line of sight from the satellite to the receiver. This anisotropy is modeled by a phase center offset from a physical reference point to the mean electrical phase center together with its corresponding elevation- and azimuth-dependent variations. Since November 2006, the IGS applies consistent absolute phase center corrections for satellite and receiver antennas (Schmid *et al.*, 2007). The current model is available at <[18]>.

[13] `http://igs.org/`
[14] `http://ids.cls.fr/`
[15] `ftp://tai.bipm.org/iers/conv2010/chapter9`
[16] `http://www.hg.tuwien.ac.at/~ecmwf1`
[17] `http://vlbi.geod.uni-bonn.de/IVS-AC/Conventions/Chapter1.html`
[18] `ftp://igs.org/igscb/station/general/igs05.atx`

References

Agnew, D.C., 2007,"Earth Tides," in *Treatise on Geophysics: Geodesy*, T.A. Herring, ed., Elsevier, New York, pp. 163–195. 2015/06/19

Andersen, O. B., 2006, see `http://www.spacecenter.dk/data/global-ocean-tide-model-1/`.

Boehm, J., Heinkelmann, R., and Schuh, H., 2007, "Short Note: A global model of pressure and temperature for geodetic applications," *J. Geod.*, **81(10)**, pp. 679–683, doi:10.1007/s00190-007-0135-3.

Bos, M. S., 2005, personal communication.

Cartwright, D. E. and Tayler, R. J., 1971, "New computations of the tide-generating potential," *Geophys. J. Roy. astr. Soc.*, **23(1)**, pp. 45–74.

Cartwright, D. E. and Edden, A. C., 1973, "Corrected tables of tidal harmonics," *Geophys. J. Roy. astr. Soc.*, **33(3)**, pp. 253–264, doi:10.1111/j.1365-246X.1973.tb03420.x.

Chelton, D. B. and Enfield, D. B., 1986, "Ocean signals in tide gauge records," *J. Geophys. Res.*, **91(B9)**, pp. 9081–9098, doi: 10.1029/JB091iB09p09081

Chen, J.L.,Wilson, C.R., Ries, J.C. and Tapley, B.D., 2013. "Rapid ice melting drives Earth's pole to the east," *Geophys. Res. Lett.*, **40**, 2625–2630, doi:10.1002/grl.50552. 2015/06/19

Desai, S. D., 2002, "Observing the pole tide with satellite altimetry," *J. Geophys. Res.*, **107(C11)**, 3186, doi:10.1029/2001JC001224.

Doodson, A. T., 1928, "The Analysis of Tidal Observations," *Phil. Trans. Roy. Soc. Lond.*, **227**, pp. 223–279, `http://www.jstor.org/stable/91217`

Eanes, R. J., 1994, "Diurnal and semidiurnal tides from TOPEX/Poseidon altimetry," paper G32B-6, presented at the Spring Meeting of the AGU, Baltimore, MD, *EOS Trans AGU*, **75**, p. 108.

Eanes R. J. and Bettadpur, S., 1995, "The CSR 3.0 global ocean tide model," *Technical Memorandum CSR-TM-95-06*, Center for Space Research, University of Texas, Austin, TX.

Egbert, G. D., Bennett, A. F., and Foreman, M. G. G., 1994, "TOPEX/Poseidon tides estimated using a global inverse model," *J. Geophys. Res.*, **99(C12)**, pp. 24821–24852, doi: 10.1029/94JC01894

Egbert, G. D., Erofeeva, S.Y., 2002, "Efficient inverse modeling of barotropic ocean tides," *J. Atmos. Ocean. Technol.*, **19(2)**, pp. 183–204.

Farrell, W. E., 1972, "Deformation of the Earth by surface loads," *Rev. Geophys. Space Phys.*, **10(3)**, pp. 761–797, doi: 10.1029/RG010i003p00761.

Francis, O. and P. Mazzega, 1990, "Global charts of ocean tide loading effects," *J. Geophys Res.*, **95(C7)**, pp. 11411–11424, doi:10.1029/JC095iC07p11411.

Gambis, D., personal communication, 2010.

Haas, R., 1996, "Untersuchungen zu Erddeformationsmodellen für die Auswertung von geodätischen VLBI-Messungen", PhD Thesis, Deutsche Geodätische Kommission, Reihe C, Heft Nr. 466, 103 pp.

Haas, R., Scherneck, H.-G., and Schuh, H., 1997, "Atmospheric loading corrections in Geodetic VLBI and determination of atmospheric loading coefficients," in *Proc. of the 12 Working Meeting on European VLBI for Geodesy and Astronomy*, Pettersen, B.R. (ed.), Honefoss, Norway, 1997, pp. 122–132.

Hartmann, T. and Wenzel, H.-G., 1995, "The HW95 tidal potential catalogue," *Geophys. Res. Lett.*, **22(24)**, pp. 3553–3556, doi: 1029/95GL03324

Hugentobler, U., 2006, personal communication.

King, M.A. and Watson, C.S., 2014, "Geodetic vertical velocities affected by recent rapid changes in polar motion," *Geophys. J.*, **99(2)**, pp. 1161–1165, doi:10.1093/gji/ggu325. 2015/06/19

Le Provost, C., Genco, M. L., Lyard, F., Vincent, P., and Canceil, P., 1994, "Spectroscopy of the world ocean tides from a finite element hydrodynamic model," *J. Geophys. Res.*, **99(C12)**, pp. 24777–24797, doi: 10.1029/94JC01381

Le Provost, C., Lyard, F., Molines, J. M., Genco, M. L., and Rabilloud, F., 1998, "A hydrodynamic ocean tide model improved by assimilating a satellite altimeter-derived data set," *J. Geophys. Res.*, **103(C3)**, pp. 5513–5529, doi: 10.1029/97JC01733

Lefèvre, F., Lyard, F. H., and Le Provost, C., 2000, "FES98: A new global tide finite element solution independent of altimetry," *Geophys. Res. Lett.*, **27(17)**, pp. 2717–2720, doi: 10.1029/1999GL011315

Lefèvre, F., Lyard, F. H., Le Provost, C., and Schrama, E.J.O., 2002, "FES99: A global tide finite element solution assimilating tide gauge and altimetric information," *J. of Atmos. Ocean. Technol.*, **19(9)**, pp. 1345–1356.

Letellier, T., 2004, "Etude des ondes de marée sur les plateaux continentaux," Thèse doctorale, Université de Toulouse III, 237pp.

MacMillan, D. S. and Gipson, J. M., 1994, "Atmospheric pressure loading parameters from Very Long Baseline Interferometry observations," *J. Geophys. Res.*, **99(B9)**, pp. 18081–18087, doi: 10.1029/94JB01190

Mathers, E. L. and Woodworth, P. L., 2001, "Departures from the local inverse barometer model observed in altimeter and tide gauge data and in a global barotropic numerical model," *J. Geophys. Res.*, **106(C4)**, pp. 6957–6972, doi: 10.1029/2000JC000241

Mathews, P. M., Buffett, B. A., and Shapiro, I. I., 1995, "Love numbers for a rotating spheroidal Earth: New definitions and numerical values," *Geophys. Res. Lett.*, **22(5)**, pp. 579–582, doi: 10.1029/95GL00161

Matsumoto, K., Takanezawa, T. and Ooe, M., 2000, "Ocean tide models developed by assimilating TOPEX/Poseidon altimeter data into hydrodynamical model: A global model and a regional model around Japan," *J. Oceanog.*, **56(5)**, pp. 567–581.

Munk, W. H. and MacDonald, G. J. F., 1960, *The Rotation of the Earth*, Cambridge Univ. Press, New York, pp. 24–25.

Nothnagel, A., 2009, "Conventions on thermal expansion modelling of radio telescopes for geodetic and astrometric VLBI ," *J. Geod.*, **83(8)**, pp. 787–792, doi: 10.1007/s00190-008-0284-z.

Petrov, L. and J.-P. Boy, 2004, "Study of the atmospheric pressure loading signal in very long baseline interferometry observations," *J. Geophys. Res.*, **109**, B03405, 14 pp., doi: 10.1029/2003JB002500.

Ponte, R. M., Salstein, D. A., and Rosen, R. D., 1991, "Sea level response to pressure forcing in a barotropic numerical model," *J. Phys. Oceanogr.*, **21(7)**, pp. 1043–1057.

Ray, R., 1999, "A global ocean tide model From TOPEX/Poseidon altimetry: GOT99.2," *NASA Technical Memorandum, NASA/TM-1999-209478*, National Aeronautics and Space Administration, Goddard Space Flight Center, Greenbelt, MD.

Ray, R. D. and R. M. Ponte, 2003, "Barometric tides from ECMWF operational analyses," *Ann. Geophys.*, **21(8)**, pp. 1897–1910, doi:10.5194/angeo-21-1897-2003.

Ries, J.C., personal communication, 2010.

Row, L. W., Hastings, D. A., and Dunbar, P. K., 1995, "TerrainBase Worldwide Digital Terrain Data," NOAA, National Geophysical Data Center, Boulder CO.

Savcenko, R., Bosch, W., 2008, "EOT08a - empirical ocean tide model from multi-mission satellite altimetry," Report No. 81, Deutsches Geodätisches Forschungsinstitut (DGFI), München, `ftp://ftp.dgfi.badw.de/pub/EOT08a/doc/EOT08a.pdf`

Schmid, R., Steigenberger, P., Gendt, G., Ge, M., and Rothacher, M., 2007, "Generation of a consistent absolute phase center correction model for GPS receiver and satellite antennas," *J. Geod.*, **81(12)**, pp. 781–798, doi:10.1007/s00190-007-0148-y.

Scherneck, H.-G., 1990, "Loading Green's functions for a continental shield with a Q-structure for the mantle and density constraints from the geoid," *Bull. d'Inform. Marées Terr.*, **108**, pp. 7775–7792.

Scherneck, H.-G., 1991, "A parameterized solid earth tide model and ocean tide loading effects for global geodetic baseline measurements," *Geophys. J. Int.*, **106(3)**, pp. 677–694, doi: 10.1111/j.1365-246X.1991.tb06339.x

Scherneck, H.-G., 1993, "Ocean tide loading: propagation of errors from the ocean tide into loading coefficients," *man. Geod.*, **18(2)**, pp. 59–71.

Scherneck, H.-G., 1999, in *Explanatory supplement to the section "Local site displacement due to ocean loading" of the IERS Conventions (1996) Chapters 6 and 7*, Schuh, H. (ed.), DGFI Report 71, pp. 19–23.

Schwiderski, E. W., 1980, "On charting global ocean tides," *Rev. Geophys. Space Phys.*, **18**(1), pp. 243–268, doi: 10.1029/RG018i001p00243

Schwiderski, E. W. and Szeto, L. T., 1981, "The NSWC global ocean tide data tape (GOTD), its features and application, random-point tide program," *NSWC-TR 81–254*, Naval Surface Weapons Center, Dahlgren, VA, 19 pp.

Shiskin, J., Young, A., Musgrave, J.C., 1967, "The X11 variant of the Census method II seasonal adjustment program," Washington DC, Technical Paper n15, Bureau of Census, US Department of Commerce.

Sun, H. P., Ducarme, B., and Dehant, V., 1995, "Effect of the atmospheric pressure on surface displacements," *J. Geod.*, **70(3)**, pp. 131–139, doi: 10.1007/BF00943688

Tamura, Y., 1987, "A harmonic development of the tide-generating potential," *Bull. d'Inform. Marées Terr.*, **99**, pp. 6813–6855.

Tregoning, P. and C. Watson, 2009, "Atmospheric effects and spurious signals in GPS analyses", *J. Geophys. Res.*, **114(B9)**, B09403, 15 pp., doi: 10.1029/2009JB006344.

van den Dool, H. M., S. Saha, J. Schemm, and J. Huang, 1997, "A temporal interpolation method to obtain hourly atmospheric surface pressure tides in Reanalysis 1979-1995," *J. Geophys. Res.*, **102(D18)**, pp. 22013–22024, doi:10.1029/97JD01571.

van den Dool, H. M., 2004, personal communication.

Wahr, J. M., 1981, "Body tides on an elliptical, rotating, elastic, and oceanless Earth," *Geophys. J. Roy. astr. Soc.*, **64(3)**, pp. 677–703.

Wahr, J. M., 1985, "Deformation induced by polar motion," *J. Geophys. Res.*, **90(B11)**, pp. 9363–9368, doi:10.1029/JB090iB11p09363.

Wahr, J. M. and Sasao, T., 1981, "A diurnal resonance in the ocean tide and the Earth's load response due to the resonant free "core nutation"," *Geophys. J. R. astr. Soc.*, **64**, pp. 747–765.

Wenzel, H.-G., 1996 "The nanogal software: Earth tide data processing package Eterna 3.3," *Bull. d'Inform. Marées Terr.*, **124**, pp. 9425–9439.

Wessel, P. and Smith, W. H. F., 1998, "New, improved version of the Generic Mapping Tools released," *EOS Trans. AGU*, **79**, 579.

Zschau, J., 1983, "Rheology of the Earth's mantle at tidal and Chandler Wobble periods," *Proc. Ninth Int. Symp. Earth Tides*, New York, 1981, Kuo, J. T. (ed.), Schweizerbart'sche Verlagsbuchhandlung, Stuttgart, pp. 605–630.